


 CrossMark  
 click for updates
Cite this: *RSC Adv.*, 2015, 5, 18523

Received 13th January 2015

Accepted 26th January 2015

DOI: 10.1039/c5ra00747j

www.rsc.org/advances

# Investigation of thresholds in laser-induced carbonization of sumanene derivatives through *in situ* observation utilizing a Raman spectroscope†

Yuhi Inada,<sup>a</sup> Toru Amaya<sup>a</sup> and Toshikazu Hirao<sup>\*ab</sup>

A useful method was demonstrated to investigate 532 nm laser energy threshold to carbonize various compounds including sumanene derivatives through *in situ* observation utilizing a micro-Raman spectrometer. It was revealed that the thresholds of sumanene derivatives are lower than those of the planar partial structures of sumanene derivatives. Moreover, [6,6]-phenyl-C<sub>61</sub>-butyric acid methyl ester (PCBM) shows a considerably lower threshold than the sumanene derivatives utilizing this method. This work can be expected to contribute toward the evolution of laser-induced carbonization-based chemistry.

## 1. Introduction

Carbon-based compounds that include a graphitic carbon lattice have been attracting considerable interest due to their wide applications such as in electrically-conductive<sup>1</sup> and catalytic<sup>2,3</sup> materials. These carbon-based compounds have been synthesized by the pyrolysis of various organic compounds, including polymers, such as polyimide and  $\pi$ -conjugated low-molecular-weight compounds, using heat sources such as electric furnaces<sup>4–10</sup> and lasers.<sup>11–30</sup> Among these sources, laser is an attractive heat source because it has advantages that other heat sources do not possess. For example, laser enables a target to be heated rapidly to a very high temperature.<sup>31</sup> In addition, a focused laser can carbonize the surface of a target in a minute region. Thus, this laser-induced carbonization is expected to be an important technique, especially for applications such as electronic devices.<sup>11,17,18,30</sup> However, systematic examination of the minimum laser energy required for carbonization (carbonization energy threshold) still remains to be studied as one of the critical factors in laser-induced carbonization. Therefore, if a fundamental method can be developed to systematically investigate the carbonization energy threshold, it will contribute toward the evolution of laser-induced carbonization-based chemistry.

Laser Raman spectroscopy is one of the best methods to confirm carbonization through the detection of the G and D bands, which are attributed to the graphitic carbon lattice and

sp<sup>3</sup>-bonded carbon or structural defects, respectively (Fig. 1a).<sup>32</sup> Therefore, we combined laser-induced carbonization with laser Raman spectroscopy, enabling us to efficiently perform the two

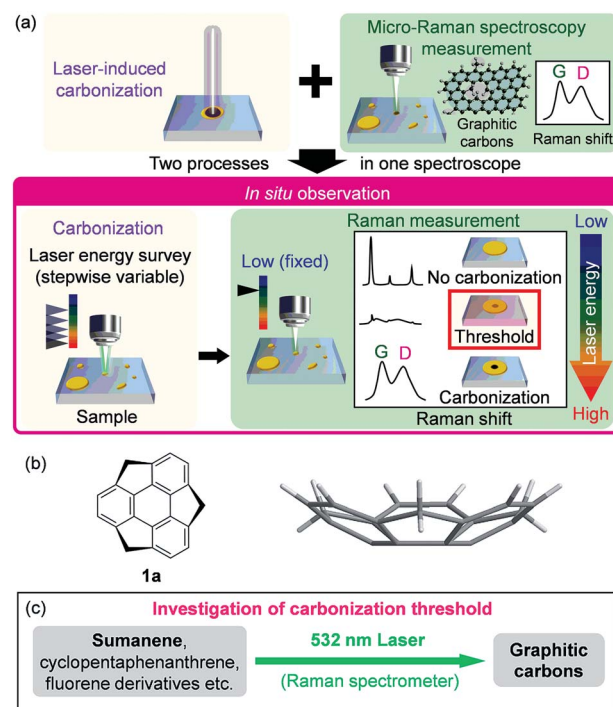


**Fig. 1** (a) Schematic illustration of *in situ* observation of laser-induced carbonization. Inset shows the schematic diagram of Raman spectra and samples after exposure to a laser for carbonization, where the detection of G and D bands depends on the laser energy for carbonization. The spectra are schematic illustrations. (b) Sumanene (1a) and its molecular structure based on X-ray crystallographic analysis.<sup>33</sup> (c) Investigation of the carbonization threshold by the *in situ* observation of laser-induced carbonization of sumanene, cyclopentaphenanthrene, fluorene derivatives etc.

<sup>a</sup>Department of Applied Chemistry, Graduate School of Engineering, Osaka University, Yamada-oka, Suita, Osaka 565-0871, Japan. E-mail: hirao@chem.eng.osaka-u.ac.jp  
<sup>b</sup>JST, ACT-C, 4-1-8 Honcho, Kawaguchi, Saitama 332-0012, Japan

† Electronic supplementary information (ESI) available: (1) FT-IR and <sup>1</sup>H and <sup>13</sup>C NMR spectra of 2b and 8, (2) raw and modified Raman spectra for *in situ* observation with a Raman spectroscope, (3) energy level diagrams and BDE values obtained by DFT calculation, experimental details for (4) thermogravimetry, and (5) thermal pyrolysis and Raman measurements of the products. See DOI: 10.1039/c5ra00747j

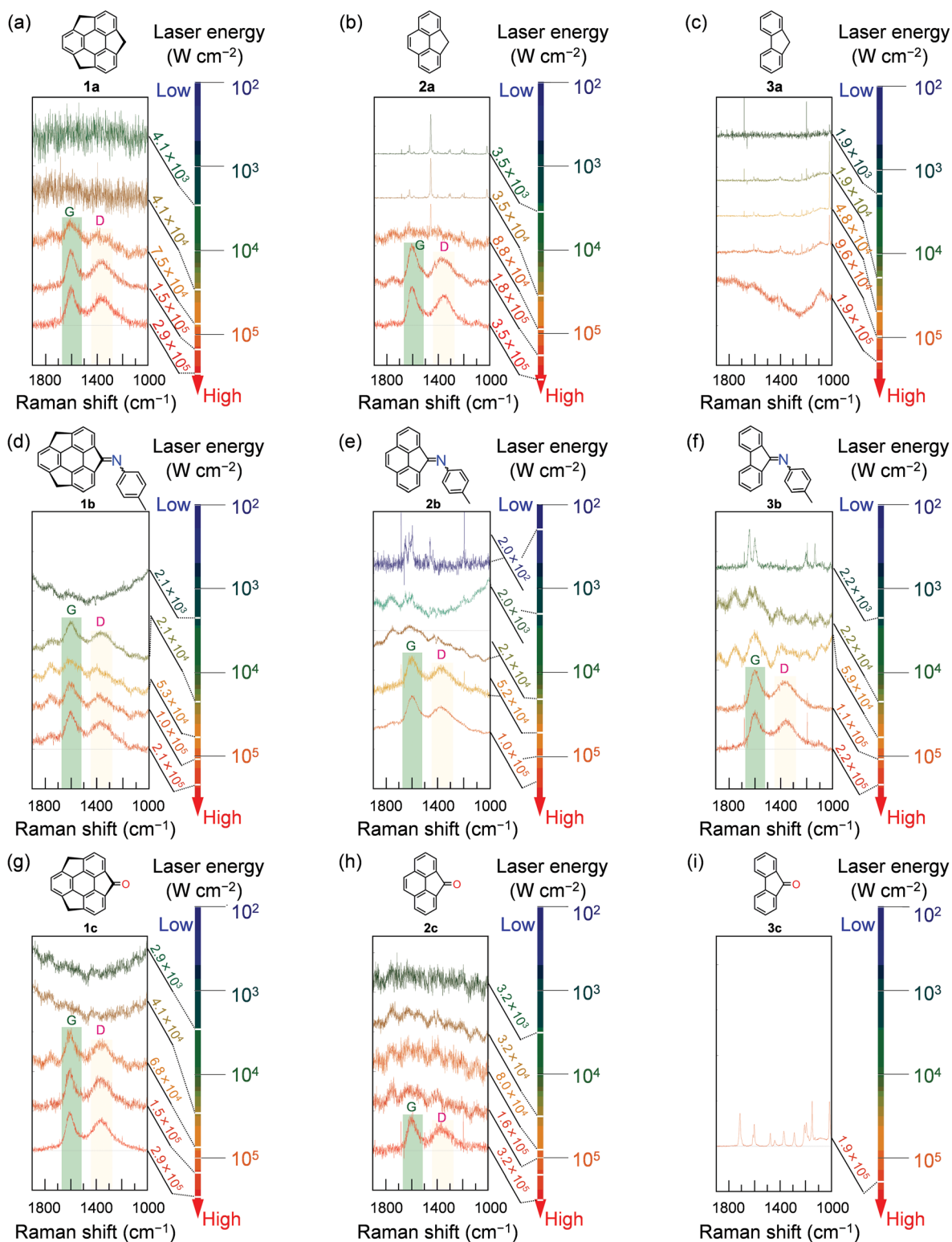


Fig. 2 Dependence of Raman spectra on 532 nm laser energy for carbonization in (a)–(c) non-substituted, (d)–(f) imino-substituted, and (g)–(i) carbonyl-substituted derivatives of sumanene, cyclopentaphenanthrene, and fluorene. The spectra are arranged in sequence as going from up to down in the order of the lowest to the highest in laser energy. G and D in the graphs denote the G and D bands, respectively. Note that all spectra are displayed after subtracting the linear background and normalizing the spectra for ease of comparison.<sup>48</sup> The raw spectra are available in Tables S1–S15.†

processes, carbonization and Raman spectroscopy measurements, simultaneously in one spectroscope (Fig. 1a). We believe that this method is very suitable for investigating carbonization energy threshold, permitting us to perform a rapid screening. In fact, Kostecki *et al.* reported the fabrication of micro electrodes through this method.<sup>27</sup> However, to the best of our knowledge, there are no reports of the investigation on the carbonization energy threshold utilizing such *in situ* observation of laser-induced carbonization.

We have been strenuously investigating the bowl-shaped  $\pi$ -conjugated molecule sumanene (**1a**) (Fig. 1b)<sup>34</sup> since its synthesis.<sup>35</sup> In our previous work, we reported the synthesis of nitrogen-doped graphitic carbons (NGCs) through laser annealing (355 nm) of sumanenemoneone imine derivatives, including **1b** (Fig. 2), while retaining the ratio of nitrogen to carbon (N/C ratio).<sup>36,37</sup> We wonder if the retention of the N/C ratio may be due to the fact that the sumanenemoneone imine derivatives can be carbonized at a lower energy than other typical compounds.<sup>38</sup> Actually, in our previous work,<sup>36</sup> no conductivity change was observed in the laser annealing of the fluorenone imine derivative **3b** (Fig. 2), a compound that has the planar partial structure of sumanenemoneone imine derivatives under the same conditions, implying that their carbonization energy thresholds differ greatly. If this significant difference results from a property of bowl-shaped molecules, we could identify a novel aspect in the properties of a  $\pi$  bowl.<sup>39</sup>

In this context, herein, we report a useful method to investigate the carbonization energy thresholds of sumanene derivatives and other compounds by *in situ* observation of their laser-induced carbonization in a micro-Raman spectrometer (Fig. 1c), which revealed that sumanene derivatives tend to have lower thresholds than the other compounds.

## 2. Experimental methods

### 2.1 Materials preparation

**2.1.1 Materials.** In this paper, compounds **1a–c**, **2a–c**, **3a–c**, and **4–9** (Fig. 3) were used for the experiments. Compounds **2a**, **3a**, **3c**, **4**, **5**, **6**, **7** and **9** were purchased from commercial sources. The other compounds used were synthesized according to the following procedures.

**2.1.2 Synthesis.** Compounds **1a**,<sup>35</sup> **1b**,<sup>36</sup> **1c**<sup>40</sup> and **3b**<sup>36</sup> were synthesized according to the previously reported procedures. The preparation of **2c**, **2b**, and **8** is described in this section.

**General.** <sup>1</sup>H (400 MHz) and <sup>13</sup>C (100 MHz) NMR spectra were measured on a JEOL JNM-ECS 400 spectrometer. CDCl<sub>3</sub> or CD<sub>2</sub>Cl<sub>2</sub> was used as a solvent. The residual CHCl<sub>3</sub> or CHDCl<sub>2</sub> peak ( $\delta = 7.26$  or  $5.32$  ppm) was used as the reference for <sup>1</sup>H NMR, respectively. The CDCl<sub>3</sub> or CD<sub>2</sub>Cl<sub>2</sub> peak ( $\delta = 77.0$  or  $53.8$  ppm) was used as the reference for <sup>13</sup>C NMR, respectively. Infrared spectra were recorded on a JASCO FT/IR-480plus spectrometer. Mass spectra were recorded on a BRUKER AUTOFLEX III (MALDI-TOF) mass spectrometer. Reagents were purchased from commercial sources and used without further purification unless otherwise indicated.

**4H-Cyclopenta[def]phenanthren-4-one (2c).** A round-bottomed flask equipped with a magnetic stirring bar was charged with

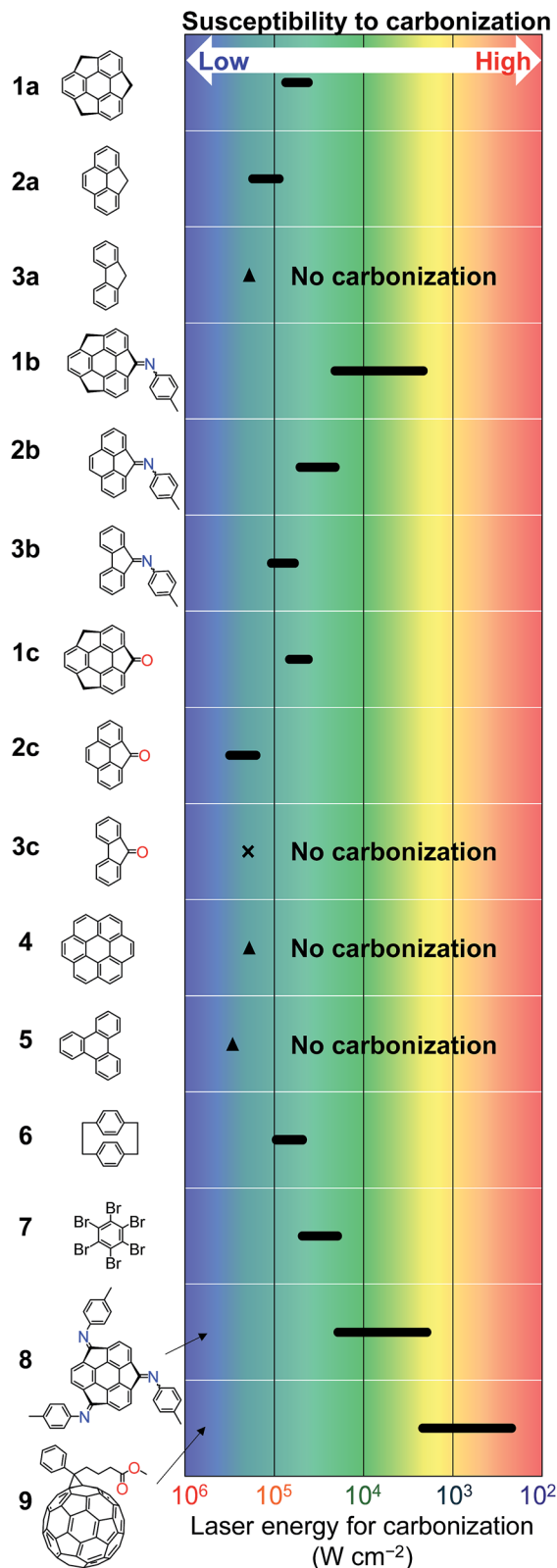
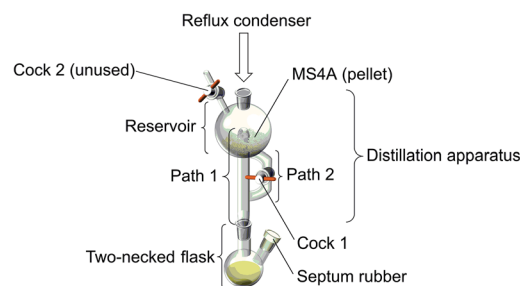


Fig. 3 532 nm laser-induced carbonization energy thresholds of compounds **1–9**. —: Threshold range, ×: no observation of G and D bands, ▲: difficult to judge whether the G and D bands were observed or not. The susceptibility to carbonization increases as the threshold range is shifted to the right.

4*H*-cyclopenta[def]phenanthrene (**2a**) (72.1 mg, 0.379 mmol), ruthenium(III) chloride hydrate (133.4 mg), pyridine (5 mL), and dichloromethane (20 mL). To the stirred reaction mixture, *t*-butyl hydroperoxide solution (70% in H<sub>2</sub>O, 1.0 mL) was added at room temperature. After stirring at room temperature for 4 days, the reaction was quenched by the addition of a solution mixture (~4 mL) [aqueous Na<sub>2</sub>S<sub>2</sub>O<sub>3</sub> solution (32 wt%)/saturated aqueous NaHCO<sub>3</sub> solution = 1/2 (volume ratio)]. The reaction mixture was poured into desalinated water and dichloromethane. The aqueous layer was extracted twice with dichloromethane. The combined organic layer was washed with 1 N HCl aqueous solution (twice) and brine, dried over Na<sub>2</sub>SO<sub>4</sub>, and evaporated *in vacuo*. The residue was purified through a short pad of silica gel (height: ~3 cm) with dichloromethane to afford the crude product (69.4 mg). The product was purified by reprecipitation (dichloromethane/methanol). After the precipitated yellow solid of **2c** was collected (17.0 mg), the filtrate was recovered. From the filtrate, the reprecipitation was performed again, and then **2c** (11.7 mg) was separated from the filtrate. Using the filtrate, further recrystallization (dichloromethane/methanol = 1/8) was carried out to yield **2c** as a yellow solid (15.0 mg). These purifications gave the pure desired compound **2c** (43.7 mg in total, 0.214 mmol, 56% yield): <sup>1</sup>H NMR (400 MHz, CDCl<sub>3</sub>): δ = 7.90 (dd, *J* = 8.0, 0.4 Hz, 2H), 7.79 (dd, *J* = 7.0, 0.4 Hz, 2H), 7.77 (s, 2H), 7.58 (dd, *J* = 8.0, 7.0 Hz, 2H) ppm [lit.,<sup>41</sup> (CDCl<sub>3</sub>): δ = 7.82 (dd, *J* = 7.5, 1.4 Hz, 2H), 7.72 (dd, *J* = 6.8, 1.4 Hz, 2H), 7.67 (s, 2H), 7.45 (dd, *J* = 7.5, 6.8 Hz, 2H) ppm]. The slight difference between the chemical shifts of our sample and the reported chemical shifts are believed to possibly arise from the concentration difference.

*N*-(*p*-Tolyl)-4*H*-cyclopenta[def]phenanthren-4-imine (**2b**). A dried reaction apparatus purged with nitrogen was equipped with a reflux condenser, a dried 20 mL two-necked flask was set with a magnetic stirring bar, and activated MS4A molecular sieves (pellets, 5.0 g) were placed in a solvent reservoir (see diagram below). After the flask was charged with 4*H*-cyclopenta[def]phenanthren-4-one (**2c**) (15.0 mg, 0.0734 mmol), *p*-toluidine (63.0 mg, 0.588 mmol, 8 eq.), and anhydrous toluene (10 mL), the mixture was stirred and heated to 130 °C. During the reaction, the following operation was repeated several times: once the solvent entirely evaporated through path 1, the solvent in the reservoir was returned to the flask from path 2 through the MS4A sieves by opening cock 1. In the first 90 min, this operation was repeated after each 30 min. In the next 80 min, this operation was repeated after each 10 min, and further *p*-toluidine (63.0 mg, 0.588 mmol, 8 eq.) was added in the fifth operation. In the final 60 min, this operation was repeated after each 30 min. Subsequently, the reaction mixture was evaporated *in vacuo* to obtain the crude product as a yellow solid (21.7 mg, 95% conversion). The residue was purified by preparative thin-layer chromatography (hexane/dichloromethane = 1/1) to afford **2b** (18.7 mg, 3% impurity) as a yellow solid. Further purification was undertaken by preparative thin-layer chromatography (hexane/ethyl acetate = 2/1) to provide **2b** (including 1% **2c**) as a yellow solid. Finally, the solid was refined by recrystallization (hexane/dichloromethane, cooling from 25 °C to -7 °C at the rate of 0.1 °C min<sup>-1</sup>) to yield the target

compound **2b** (4.2 mg, 0.0143 mmol, including 1% **2c**) as needle-like yellow crystals: FT-IR (ATR, powder): ν = 3053, 2918, 2855, 1621, 1504 cm<sup>-1</sup> (Fig. S1†); <sup>1</sup>H NMR (400 MHz, CDCl<sub>3</sub>): δ = 8.02 (d, *J* = 7.1 Hz, 1H), 7.89 (d, *J* = 8.0 Hz, 1H), 7.82–7.71 (m, 3H), 7.66 (m, 1H), 7.30–7.24 (m, 3H), 7.03 (d, *J* = 8.0 Hz, 2H), 6.74 (d, *J* = 7.3 Hz, 1H), 2.46 (s, 3H) ppm (Fig. S2†); <sup>13</sup>C NMR (100 MHz, CDCl<sub>3</sub>): δ = 164.61, 149.28, 138.46, 137.78, 136.21, 134.26, 130.48, 130.00, 128.78, 128.13, 128.10, 127.77, 127.65, 127.43, 125.35, 124.97, 121.08, 119.00, 21.23 ppm (because these results lack one peak, two peaks are considered to be accidentally coincident; Fig. S3†); HRMS (MALDI-TOF): *m/z* calcd for C<sub>22</sub>H<sub>15</sub>N [M<sup>+</sup>] 293.1199, found 293.1188.



*Sumanetrione triimine* **8**. Trioxosumanene<sup>40</sup> (10.3 mg, 33.6 μmol) and *p*-toluidine (21.6 mg, 20.2 μmol, 6 eq.) were charged into a dried round-bottomed flask equipped with a magnetic stirring bar and activated molecular sieves (MS4A, pellets, 0.5 g). After evacuation followed by purging with argon, 10 mL of absolute toluene was added to the mixture. The reaction mixture was heated to 120 °C and stirred for 4 h under argon. After the addition of activated molecular sieves (MS4A, pellets, 0.5 g) again to the reaction mixture under argon, the mixture was stirred for 14 h under argon at 120 °C. The reaction mixture was cooled to ambient temperature, and then filtered through cotton. The filtrate was evaporated *in vacuo*. The residue was purified by preparative thin-layer chromatography (dichloromethane) to obtain the desired compound **8** as a red-orange solid. Furthermore, the solid was refined by reprecipitation (dichloromethane/cooled hexane) to provide **8** (6.5 mg, 11.3 μmol, 34%) as needle-like red-orange crystals: FT-IR (KBr): ν = 3023, 2921, 2856, 1891, 1719, 1648, 1618, 1560, 1502, 1392, 1327, 1194, 1108, 1016 cm<sup>-1</sup> (Fig. S4†); <sup>1</sup>H NMR (400 MHz, CD<sub>2</sub>Cl<sub>2</sub>): δ = 7.62 (d, *J* = 7.7 Hz, 1H), 7.60 (d, *J* = 7.7 Hz, 1H), 7.32–7.21 (m, 6H), 7.21–7.14 (m, 6H), 7.11 (d, *J* = 8.2 Hz, 2H), 7.04 (d, *J* = 8.2 Hz, 2H), 6.99 (d, *J* = 8.2 Hz, 2H), 6.51 (d, *J* = 7.9 Hz, 1H), 6.98 (d, *J* = 7.9 Hz, 1H), 6.10 (d, *J* = 7.9 Hz, 1H), 6.07 (d, *J* = 7.9 Hz, 1H), 2.45 (s, 3H), 2.43 (s, 3H), 2.37 (s, 3H), 2.36 (s, 3H) ppm (Fig. S5†); <sup>13</sup>C NMR (100 MHz, CD<sub>2</sub>Cl<sub>2</sub>): δ = 163.05, 163.01, 162.92, 162.87, 148.94, 148.76, 148.47, 148.44, 148.37, 148.30, 148.29, 148.27, 148.19, 148.16, 147.93, 147.87, 146.36, 146.04, 145.86, 145.50, 139.77, 139.55, 139.37, 139.11, 136.32, 136.30, 136.17, 136.13, 130.24, 130.22, 130.10, 130.09, 126.78, 126.64, 126.60, 126.52, 124.88, 124.81, 124.66, 124.63, 120.96, 120.90, 120.76, 120.70, 21.21, 21.20, 21.12, 21.11 ppm (Fig. S6†); HRMS (MALDI-TOF): *m/z* calcd for C<sub>42</sub>H<sub>28</sub>N<sub>3</sub><sup>+</sup> [M + H]<sup>+</sup> 574.2278, found 574.2275.

## 2.2 Materials characterization

**2.2.1 Sample preparation.** Each compound (~1 mg) was generally dissolved in 100  $\mu\text{L}$  of dichloromethane (toluene was used for **9**). The solution (~5  $\mu\text{L}$ ) was drop-cast onto a glass substrate. After drying in air, it was further dried *in vacuo*. The solvents were commercially available and employed without further purification.

**2.2.2 Carbonization and Raman measurements.** To investigate the energy thresholds in the laser-induced carbonization of the above-mentioned samples, a green continuous-wave laser (532 nm) equipped in a micro-Raman spectrometer (JASCO, NRS-3100) was utilized not only as the exciting source for Raman measurements but also as the heat source for carbonization. The laser energy can be monitored at any time and controlled stepwise through a neutral density (ND) filter with optical densities (OD) of 3, 2, 1, 0.6, and 0.3, which can be manually switched using the software. In the case when an ND filter was not inserted, the value of OD was represented as 0. The laser output energy depends on the ambient conditions. The laser beam can be focused through an objective lens (20 or 100 times), where the beam diameters are ~4 or ~1  $\mu\text{m}$ , respectively. The incident power of the laser was monitored between an ND filter and the objective lens using a power meter that is incorporated in the Raman spectrometer. The laser energy under the objective lens was calculated by dividing the as-obtained power of the laser by the beam waist area.

First, each sample was mounted onto the stage of the micro-Raman spectrometer. Numerous particles with various sizes were observed through the microscope of the spectrometer in each sample. Note that the particle size chosen for the measurement should be similar in size to the laser beam diameter because it affects the spectrum after the sample is exposed to the laser. In fact, if the particle was too large, the signal derived from the carbonized region was buried within that of an intrinsic region. In contrast, if the particle was very small, the signal was too small to be detected. In particular, when a sample emits fluorescence resulting from excitation by the laser, the particle should be carefully chosen such that the signal obtained from the carbonized region is not buried due to the fluorescence.

Second, each sample was exposed to a laser under the conditions for carbonization, as shown in Tables S1–S15.† Then, the spectra after laser exposure were obtained under the conditions for Raman measurement, as listed in Tables S1–S15.† The laser energy for the measurements was carefully chosen such that it does not exceed that required for carbonization. The raw spectra were modified by subtracting the linear background and normalizing the spectra to easily locate the G and D bands (~1600 and ~1360  $\text{cm}^{-1}$ , respectively) and compare them with each other. The modification was undertaken using an analysis software (JASCO, Spectra Manager Version 2).

Third, a judgment was performed regarding whether the G and D bands could be detected. The results are listed in Tables S1–S15,† where the denotations  $\times$ ,  $\blacktriangle$ , and  $\circ$  were used in the cases when the G and D bands were not detected, when it was

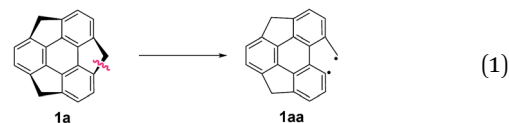
difficult to judge the detection of the G and D bands, and when the G and D bands were clearly detected, respectively.

Finally, the carbonization energy threshold was determined as the range of the laser energy corresponding to the region between  $\blacktriangle$  and  $\circ$  or between  $\times$  and  $\circ$ . The results are visualized in Fig. 3.

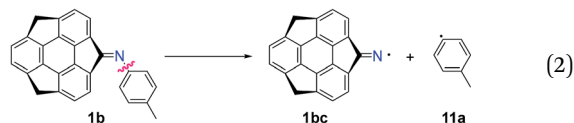
## 2.3 Density functional theory (DFT) calculation

To estimate the bond dissociation energy (BDE), energy levels of the various species were calculated by the density functional theory (DFT) method using the Gaussian 09 program.<sup>42</sup> The vibrational analysis was performed after the optimization of the molecular structures. For both the vibrational analysis and structure optimization, the hybrid functional and basis sets were B3LYP/6-31G(d,p) and UB3LYP/6-31+G(d,p) for the closed-shell and open-shell molecules, respectively.

**2.3.1 Calculation of BDEs.** Table S16† summarizes the sums of the electronic and zero-point energies ( $E$ ) for each species.  $E$  of species **n** is denoted by  $E_n$ . Based on these results, the BDEs of various bonds were calculated by subtracting the  $E$  of the species before bond dissociation from that after bond dissociation [see an example in eqn (1)]. In the case that two species were generated through bond dissociation, the  $E$  of the species before bond dissociation was subtracted from the sum of  $E$  after bond dissociation [see an example in eqn (2)]. These results are also listed in Table S16.†



$$\text{BDE}(\text{Ar-CH}_2 \text{ in } \mathbf{1a}) = E_{\mathbf{1aa}} - E_{\mathbf{1a}}$$



$$\text{BDE}(\text{C=N-Tol in } \mathbf{1b}) = E_{\mathbf{1bc}} + E_{\mathbf{11a}} - E_{\mathbf{1b}}$$

**2.3.2 Estimation of strain energy of sumanene.** As described in the results and discussion section, the Ar-CH<sub>2</sub> bond in sumanene (**1a**) shows a considerably lower BDE than that of cyclopentaphenanthrene **2a** and fluorene **3a** [125 (**1a**)  $\ll$  327 (**2a**) < 376  $\text{kJ mol}^{-1}$  (**3a**)] (see Table S16†). These results can be explained by the strain energy inherent in sumanene (**1a**), as shown in Fig. S7a.† The structure of *bowl-shaped* biradical **1ab** was optimized to obtain a *planar* biradical **1aa**. When the structure of **1ab** changes from *bowl-shaped* to planar, its strain energy can be released. As a result,  $E_{\mathbf{1ab}}$  was decreased by the

strain energy, which results in a lowering of the BDE. If  $E_{1ab}$  can be calculated, the strain energy can be directly estimated (Fig. S7a†). However, it is difficult to calculate  $E_{1ab}$  because the structure optimization of *bowl-shaped* biradical **1ab** produced *planar* biradical **1aa**, as described above. If the BDE of *unstrained sumanene* can be calculated, the strain energy can be directly estimated, but such a compound cannot be obtained. Instead of this *unstrained* compound, 1,7-dimethyl-4*H*-cyclopenta[def]triphenylene (**10**, Fig. S7b†) was designed. The structure of **10** corresponds to that where two Ar-CH<sub>2</sub> bonds in sumanene (**1a**) are dissociated to possess an *unstrained* structure. The strain energy can be estimated as 164 kJ mol<sup>-1</sup> by subtracting the BDE (Ar-CH<sub>2</sub>) of **1a** ( $E_{1aa} - E_{1a} = 125$  kJ mol<sup>-1</sup>) from that of **10** ( $E_{10a} - E_{10} = 289$  kJ mol<sup>-1</sup>).

**2.3.3 Calculation of temperature increase corresponding to strain energy in sumanene.** To intuitively grasp the extent to which the strain energy of sumanene (**1a**) supports the carbonization, the strain energy (164 kJ mol<sup>-1</sup>) was converted to the temperature increase of **1a**. Note that the results of this calculation do not indicate the actual temperature increase. The estimation includes the following assumptions. (1) Specific heat capacity was fixed at a constant value, although this value depends on the temperature. (2) The melting and/or decomposition of **1a** does not occur even when the temperature has reached an actual melting and/or decomposition point. For these reasons, the estimated temperature increase is a maximum value. The specific heat capacity at constant pressure ( $C_p$ ) was calculated as 247 J mol<sup>-1</sup> K<sup>-1</sup> at 298.15 K, which was derived from the specific heat capacity at constant volume ( $C_v = 57$  cal mol<sup>-1</sup> K<sup>-1</sup>) obtained by DFT calculation and Mayer's relation ( $C_p = C_v + R$ , where  $R$  represents the gas constant). Therefore, the strain energy (164 kJ mol<sup>-1</sup>) divided by  $C_v$  (57 cal mol<sup>-1</sup> K<sup>-1</sup>) gives the temperature increase (660 K). Moreover, for both structure optimization and vibrational analysis, B3LYP/6-31G(d,p) was used as the hybrid functional and basis set.

### 3. Results and discussion

We employed a micro-Raman spectrometer with an objective lens and continuous-wave laser (532 nm) as an exciting source, allowing microscope observation and Raman spectral measurement of the target compound in a minute region (Fig. 1). Moreover, the laser energy can be controlled stepwise with software through neutral density filters incorporated in the spectroscope. Generally, considerable attention must be paid to the laser energy because a high-energy laser can damage a sample. Here, the laser was utilized not only as the exciting source for micro-Raman spectroscopy measurement, but also as the heating source for carbonization, by appropriately adjusting the laser energy (Fig. 1).

Fig. 2 shows the dependence of the Raman spectra on the 532 nm laser energy for carbonization of nine compounds, including sumanene derivatives. The laser energy threshold to detect the G and D bands is summarized in Fig. 3. First, we checked the carbonization energy threshold of sumanene (**1a**) and the compounds **2a** and **3a** with their planar partial structures. The results of the laser-induced carbonization of **1a** are

shown in Fig. 2a. The Raman spectra signals after exposing **1a** to a lower-energy laser ( $4.1 \times 10^3$  and  $4.1 \times 10^4$  W cm<sup>-2</sup>) for 1 min were too weak to be clearly observed. As the laser energy for carbonization was increased ( $7.5 \times 10^4$ ,  $1.5 \times 10^5$ , and  $2.9 \times 10^5$  W cm<sup>-2</sup>), G and D bands were clearly detected. The spectrum after laser exposure ( $2.9 \times 10^5$  W cm<sup>-2</sup>) is similar to that formed by heating to approximately 600–1500 °C.<sup>6,43–47</sup> In this case, the range of the carbonization energy threshold for **1a** was determined to be  $4.1 \times 10^4$  to  $7.5 \times 10^4$  W cm<sup>-2</sup> (**1a** in Fig. 3). On the other hand, in the case of cyclopentaphenanthrene **2a**, its intrinsic spectra were observed when the laser energy for carbonization fell below  $3.5 \times 10^4$  W cm<sup>-2</sup> (Fig. 2b). In the next step ( $8.8 \times 10^4$  W cm<sup>-2</sup>), the intrinsic peaks disappeared, suggesting that **2a** was damaged due to the laser exposure. Further enhancement of the laser energy ( $1.8 \times 10^5$  and  $3.5 \times 10^5$  W cm<sup>-2</sup>) resulted in obvious G and D bands, showing that the threshold exists over the range from  $8.8 \times 10^4$  to  $1.8 \times 10^5$  W cm<sup>-2</sup>. Regarding the similar compound **3a** (Fig. 2c), G and D bands were not detected even though the laser worked at full power ( $1.9 \times 10^5$  W cm<sup>-2</sup>), and the intrinsic peaks vanished. These results show that the threshold increases in the order of sumanene **1a** < cyclopentaphenanthrene **2a** < fluorene **3a**. This order is in accordance with the increase of the lowest bond dissociation energy (BDE) among the bonds included in each compound, where the lowest BDE was estimated by density functional theory (DFT) calculation [Ar-CH<sub>2</sub>: 125 (**1a**) < 327 (**2a**) < 376 kJ mol<sup>-1</sup> (**3a**)] (see Table S16†). The BDE of sumanene (**1a**) is considerably lower than of the other compounds, which is clearly induced by its inherent strain energy. The strain energy was estimated by DFT calculation to be 164 kJ mol<sup>-1</sup> (see Experimental section 2.3.2 for details). If the whole strain energy is assumed to contribute toward the increase of temperature in solid **1a** after the bond dissociation, the strain energy can be converted to the temperature increase by ~660 °C<sup>49</sup> (see Experimental section 2.3.3 for details), which may also support the results mentioned above. Although these compounds have virtually no light absorption at 532 nm, at least in a solution state,<sup>50–52</sup> it has been suggested that they absorb 532 nm light in a solid state and/or multiphoton absorption<sup>53,54</sup> occurs.

Next, similar experiments were performed considering imines **1b**, **2b**, and **3b** and ketones **1c**, **2c**, and **3c**. The results are summarized in Fig. 2d–i. When the substituent (C=N-Tol or C=O) is fixed, the order of the threshold exhibits the same tendency (**1b** < **2b** < **3b** and **1c** < **2c** < **3c**) as the above-mentioned non-substituted compounds (**1a** < **2a** < **3a**). These results are consistent with those of the laser-induced carbonization (355 nm) of **1b** and **3b**, which were reported in our previous work as described in the introduction. In contrast, when the skeleton of the compound (sumanene, cyclopentaphenanthrene, or fluorene) is fixed, the threshold range tends to increase in the following order (**nb** < **nc** < **na**,  $n = 1–3$ ). This tendency may also be accounted for by the increase of each lowest BDE [95 (**1b**: Ar-CH<sub>2</sub>) < 111 (**1c**: Ar-CH<sub>2</sub>) < 125 (**1a**: Ar-CH<sub>2</sub>), 253 (**2b**: Ar-C=N) < 284 (**2c**: Ar-C=O) < 327 (**2a**: Ar-CH<sub>2</sub>), 273 (**3b**: N-Tol) < 327 (**3c**: Ar-C=O) < 376 kJ mol<sup>-1</sup> (**3a**: Ar-CH<sub>2</sub>)] (see Table S16†). The efficiency of light absorption can also be included as one of the

other factors affecting the results. Indeed, 532 nm light absorption in the solid state is observed in **1b**<sup>36</sup> but is not in **1a**.<sup>51</sup>

Furthermore, to demonstrate the further scope of the presented method, additional experiments were performed for six additional compounds as follows (Fig. 3): coronene (**4**), triphenylene (**5**), [2.2]paracyclophane (**6**), hexabromobenzene (**7**), sumanenetrione triimine **8**, and [6,6]-phenyl-C<sub>61</sub>-butyric acid methyl ester (PCBM, **9**). The carbonization energy thresholds are summarized in Fig. 3 for all the compounds that were studied in this paper. Non-substituted compounds **4** and **5** could not be carbonized, even when the laser energy was increased to the maximum value ( $1.9 \times 10^5$  and  $2.9 \times 10^5$  W cm<sup>-2</sup>, respectively), implying that the introduction of substituents is likely important to reduce the threshold. Furthermore, cyclophane **6**, which bears four methylene carbons, was employed to observe its carbonization at the laser energy of  $1.9 \times 10^5$  W cm<sup>-2</sup>. In the case of hexabromobenzene (**7**), which has weaker bonds, carbonization occurred under the lower laser-energy conditions ( $4.9 \times 10^4$  W cm<sup>-2</sup>) than for **6**. Sumanenetrione triimine **8**, which contains more imino groups than sumanenemoneone **1c**, showed a similar threshold range to **1c**. Finally, PCBM (**9**) was tested as well, and was found to have the lowest threshold range ( $2.2 \times 10^2$  to  $2.2 \times 10^3$  W cm<sup>-2</sup>) among all the candidates studied in this paper. This might be due to reasons such as inherent high strain and/or good absorption of visible light<sup>55,56</sup> in the fullerene derivative. Because the UV<sup>16,22,30</sup> or NIR<sup>21</sup> laser-induced carbonization of fullerene itself has been already known, it was interesting to find that fullerene derivative **9** was carbonized by 532 nm laser using the presented method.

## 4. Conclusions

In summary, the *in situ* observation of laser-induced carbonization for fifteen compounds revealed that sumanene derivatives tend to possess the lower carbonization energy thresholds than the corresponding planar compounds with the partial structures. Moreover, PCBM was found to have a considerably lower threshold than the sumanene derivatives utilizing the present method. We expect this report to be useful for systematically investigating the carbonization energy thresholds in various compounds, leading to contributions toward the development of laser-induced carbonization-based chemistry.

## Acknowledgements

We thank Prof. Nobuhito Imanaka and Dr Toshiyuki Masui for the Raman measurements. We also express our appreciation to Dr Ichiro Hisaki for the TG measurements. This work was partially supported by Grants-in-Aid for Scientific Research (A) (22245007) and Young Scientists (A) (22685006) from JSPS. Financial support from JST (ACT-C) is also acknowledged. Y.I. expresses special thanks to a JSPS fellowship for young scientists.

## Notes and references

1 D. D. L. Chung, *J. Mater. Sci.*, 2004, **39**, 2645–2661.

- 2 E. Antolini, *Appl. Catal., B*, 2012, **123–124**, 52–68.
- 3 H. Wang, T. Maiyalagan and X. Wang, *ACS Catal.*, 2012, **2**, 781–794.
- 4 S. D. Bruck, *Polymer*, 1965, **6**, 319–332.
- 5 M. Murakami, H. Yasujima, Y. Yumoto, S. Mizogami and S. Yoshimura, *Solid State Commun.*, 1983, **45**, 1085–1088.
- 6 T. Ohnishi, I. Murase, T. Noguchi and M. Hirooka, *Synth. Met.*, 1987, **18**, 497–502.
- 7 Y. B. Roh, H. Araki, K. Yoshino, M. Takase and T. Banjyo, *Jpn. J. Appl. Phys., Part 1*, 1994, **33**, 1146–1152.
- 8 J. R. Pels, F. Kapteijn, J. A. Moulijn, Q. Zhu and K. M. Thomas, *Carbon*, 1995, **33**, 1641–1653.
- 9 R. Liu, D. Wu, X. Feng and K. Müllen, *Angew. Chem.*, 2010, **122**, 2619–2623.
- 10 R. Liu, D. Wu, X. Feng and K. Müllen, *Angew. Chem., Int. Ed.*, 2010, **49**, 2565–2569.
- 11 J. I. Raffel, J. F. Freidin and G. H. Chapman, *Appl. Phys. Lett.*, 1983, **42**, 705–706.
- 12 C. Decker, *J. Polym. Sci., Part C: Polym. Lett.*, 1987, **25**, 5–10.
- 13 M. Schumann, R. Sauerbrey and M. C. Smayling, *Appl. Phys. Lett.*, 1991, **58**, 428–430.
- 14 S. Kawanishi, Y. Shimizu, S. Sugimoto and N. Suzuki, *Polymer*, 1991, **32**, 979–983.
- 15 A. Ouchi and A. Yabe, *Jpn. J. Appl. Phys., Part 1*, 1992, **31**, 1295–1298.
- 16 H. M. Phillips, D. Sarkar, N. J. Halas, R. H. Hauge and R. Sauerbrey, *Appl. Phys. A: Solids Surf.*, 1993, **57**, 105–107.
- 17 R. Srinivasan, R. R. Hall and D. C. Allbee, *Appl. Phys. Lett.*, 1993, **63**, 3382–3383.
- 18 R. Srinivasan, R. R. Hall, W. D. Wilson, W. D. Loehle and D. C. Allbee, *Synth. Met.*, 1994, **66**, 301–307.
- 19 H. Tsubakihara, M. Takeda, K. Okada and A. Sakamoto, *Kobunshi Ronbunshu*, 1994, **51**, 361–363.
- 20 M. Yudasaka, Y. Tasaka, M. Tanaka, H. Kamo, Y. Ohki, S. Usami and S. Yoshimura, *Appl. Phys. Lett.*, 1994, **64**, 3237–3239.
- 21 M. Ferretti, A. Parisini, M. Manfredini and P. Milani, *Chem. Phys. Lett.*, 1996, **259**, 432–437.
- 22 D. Ning, Q. H. Lou, J. X. Dong and Y. R. Wei, *Appl. Phys. A*, 1996, **62**, 509–512.
- 23 S. Nishio, *J. Photopolym. Sci. Technol.*, 1997, **10**, 175–180.
- 24 M. Endo, N. Kota, S. Ishibe, M. Ueda, K. Oshida and T. Kasai, *J. Inst. Electr. Eng. Jpn.*, 1997, **117**, 638–644.
- 25 T. Lippert, E. Ortelli, J. C. Panitz, F. Raimondi, J. Wambach, J. Wei and A. Wokaun, *Appl. Phys. A*, 1999, **69**, S651–S654.
- 26 Z. Qin, X. Huang, D. Wang, T. He, Q. Wang and Y. Zhang, *Surf. Interface Anal.*, 2000, **29**, 514–518.
- 27 R. Kostecki, X. Song and K. Kinoshita, *Electrochem. Solid-State Lett.*, 2002, **5**, E29–E31.
- 28 K. Tono, H. Kondoh, Y. Hamada, T. Suzuki, K. Bito, T. Ohta, S. Sato, H. O. Hamaguchi, A. Iwata and H. Kuroda, *Jpn. J. Appl. Phys., Part 1*, 2005, **44**, 7561–7567.
- 29 Y. Ji and Y. Jiang, *Appl. Phys. Lett.*, 2006, **89**, 221103.
- 30 J. I. Inoue, H. Wada and T. Mori, *Jpn. J. Appl. Phys.*, 2010, **49**, 0716051–0716055.
- 31 Z. Y. Qin, B. Y. Du, J. Zhang, T. B. He, L. Qin and Y. S. Zhang, *Appl. Phys. A*, 2001, **72**, 711–715.

- 32 H. C. Tsai and D. B. Bogy, *J. Vac. Sci. Technol., A*, 1987, **5**, 3287–3312.
- 33 H. Sakurai, T. Daiko, H. Sakane, T. Amaya and T. Hirao, *J. Am. Chem. Soc.*, 2005, **127**, 11580–11581.
- 34 T. Amaya and T. Hirao, *Chem. Commun.*, 2011, **47**, 10524–10535.
- 35 H. Sakurai, T. Daiko and T. Hirao, *Science*, 2003, **301**, 1878.
- 36 Y. Inada, T. Amaya, Y. Shimizu, A. Saeki, T. Otsuka, R. Tsuji, S. Seki and T. Hirao, *Chem.-Asian J.*, 2013, **8**, 2569–2574.
- 37 T. Amaya, Y. Inada, Y. Shimizu, A. Saeki, R. Tsuji, S. Seki and T. Hirao, *Chem.-Asian J.*, 2014, **9**, 2568–2575.
- 38 It was reported that a trade-off relationship exists between the degree of carbonization and the amount of nitrogen atoms in NGC because nitrogen atoms are eliminated from the graphitic carbon lattice above  $\sim 600$  °C. See ref. 7 and 18.
- 39 We refer to the bowl-shaped  $\pi$ -conjugated compounds as “ $\pi$  bowls”, whereas they have been also called open geodesic polyarenes or buckybawls. See: L. T. Scott, H. E. Bronstein, D. V. Preda, R. B. M. Ansems, M. S. Bratcher and S. Hagen, *Pure Appl. Chem.*, 1999, **71**, 209–219; P. W. Rabideau, A. H. Abdourazak, H. E. Folsom, Z. Marcinow, A. Sygula and R. Sygula, *J. Am. Chem. Soc.*, 1994, **116**, 7891–7892.
- 40 T. Amaya, M. Hifumi, M. Okada, Y. Shimizu, T. Moriuchi, K. Segawa, Y. Ando and T. Hirao, *J. Org. Chem.*, 2011, **76**, 8049–8052.
- 41 G. Sugowdz, P. J. Collin and W. H. F. Sasse, *Tetrahedron Lett.*, 1969, **10**, 3843–3846.
- 42 M. J. Frisch, G. W. Trucks, H. B. Schlegel, G. E. Scuseria, M. A. Robb, J. R. Cheeseman, G. Scalmani, V. Barone, B. Mennucci, G. A. Petersson, H. Nakatsuji, M. Caricato, X. Li, H. P. Hratchian, A. F. Izmaylov, J. Bloino, G. Zheng, J. L. Sonnenberg, M. Hada, M. Ehara, K. Toyota, R. Fukuda, J. Hasegawa, M. Ishida, T. Nakajima, Y. Honda, O. Kitao, H. Nakai, T. Vreven, J. A. Montgomery Jr, J. E. Peralta, F. Ogliaro, M. Bearpark, J. J. Heyd, E. Brothers, K. N. Kudin, V. N. Staroverov, R. Kobayashi, J. Normand, K. Raghavachari, A. Rendell, J. C. Burant, S. S. Iyengar, J. Tomasi, M. Cossi, N. Rega, J. M. Millam, M. Klene, J. E. Knox, J. B. Cross, V. Bakken, C. Adamo, J. Jaramillo, R. Gomperts, R. E. Stratmann, O. Yazyev, A. J. Austin, R. Cammi, C. Pomelli, J. W. Ochterski, R. L. Martin, K. Morokuma, V. G. Zakrzewski, G. A. Voth, P. Salvador, J. J. Dannenberg, S. Dapprich, A. D. Daniels, Ö. Farkas, J. B. Foresman, J. V. Ortiz, J. Cioslowski and D. J. Fox, *Gaussian 09, Revision C.01*, Gaussian, Inc., Wallingford CT, 2009.
- 43 M. Nakamizo, R. Kammereck and P. L. Walker Jr, *Carbon*, 1974, **12**, 259–267.
- 44 M. Endo, K. Hakamada, C. Kim, N. Miyazawa and T. Kasai, *Tanso*, 1998, **183**, 156–161.
- 45 In thermogravimetry for **1b**, as the temperature increased from room temperature to 500 °C, gradual weight loss was observed from room temperature to yield a black solid. Experimental details regarding the thermogravimetry (TG) and the obtained TG curve (Fig. S8†) are given in the ESI† [page S24, (4) thermogravimetry].
- 46 In the case of using short laser pulses at the fluence of 44 mJ cm<sup>-2</sup> (per pulse), the carbonization of **1b** was induced and confirmed by Raman and XPS analysis: see ref. 36.
- 47 The Raman spectra of the laser-annealed film of **1b** in Fig. 2d possesses G and D bands in similar positions ( $\sim 1600$  and  $\sim 1380$  cm<sup>-1</sup>) to that of the heat-treated film of **1b** at 600 °C (1603 and 1367 cm<sup>-1</sup>). Among graphitic, amorphous carbon, and nanocrystalline graphite, the positions of the G bands are considered to be assigned not to those of graphite (1581 cm<sup>-1</sup>) or amorphous carbon ( $\sim 1510$  cm<sup>-1</sup>) but to that of nanocrystalline graphite ( $\sim 1600$  cm<sup>-1</sup>). ESI† [page S24–25, (5) thermal pyrolysis and Raman measurements of the products] includes the experimental details and Raman spectra for the pristine and pyrolyzed films of **1b** (Fig. S9†).
- 48 In the Raman spectra with a sloped baseline due to a luminescence phenomenon (for example in Fig. 2h with a laser energy of 3.2 and 8.0  $\times 10^4$  W cm<sup>-2</sup>), note that the oscillations observed are not modes of vibration.
- 49 Note that the results of this calculation do not give the actual temperature increase, but are simply an attempt to intuitively grasp how much the strain energy of sumanene supports the carbonization. Moreover, the estimated temperature increase can be considered to be a maximum value; see ESI† for details.
- 50 T. Horaguchi, R. Yamazaki and T. Abe, *Bull. Chem. Soc. Jpn.*, 1980, **53**, 494–497.
- 51 T. Amaya, S. Seki, T. Moriuchi, K. Nakamoto, T. Nakata, H. Sakane, A. Saeki, S. Tagawa and T. Hirao, *J. Am. Chem. Soc.*, 2009, **131**, 408–409.
- 52 L. Giribabu, K. Sudhakar, G. Sabapathi and R. K. Kanaparthi, *J. Photochem. Photobiol., A*, 2014, **284**, 18–26.
- 53 W. Kaiser and C. G. B. Garrett, *Phys. Rev. Lett.*, 1961, **7**, 229–231.
- 54 Y. H. Pao and P. M. Rentzepis, *J. Chem. Phys.*, 1965, **43**, 1281–1286.
- 55 K. Kuhnke, M. Epple and K. Kern, *Chem. Phys. Lett.*, 1998, **294**, 241–247.
- 56 M. Murata, Y. Morinaka, Y. Murata, O. Yoshikawa, T. Sagawa and S. Yoshikawa, *Chem. Commun.*, 2011, **47**, 7335–7337.